Hyperspectral Terrain Classification for Ground Vehicles

Christian Winkens, Florian Sattler and Dietrich Paulus
University of Koblenz-Landau, Institute for Computational Visualistics, Universitätsstr. 1, 56070 Koblenz, Germany
{*cwinkens, sflorian92, paulus*}*@uni-koblenz.de*

Keywords: Hyperspectral Imaging, Terrain Classification, Spectral Analysis, Autonomous Robots.

Abstract: Hyperspectral imaging increases the amount of information incorporated per pixel in comparison to normal RGB color cameras. Conventional spectral cameras as used in satellite imaging use spatial or spectral scanning during acquisition which is only suitable for static scenes. In dynamic scenarios, such as in autonomous driving applications, the acquisition of the entire hyperspectral cube at the same time is mandatory. We investigate the eligibility of novel snapshot hyperspectral cameras. It captures an entire hyperspectral cube without requiring moving parts or line-scanning. The sensor is tested in a driving scenario in rough terrain with dynamic scenes. Captured hyperspectral data is used for terrain classification utilizing machine learning techniques. The multi-class classification is evaluated against a novel hyperspectral ground truth dataset specifically created for this purpose.

1 INTRODUCTION

Spectral imaging is an important and fast growing topic in remote sensing. It is defined by acquiring light intensity (radiance) for pixels in an image. Each pixel stores a vector of intensity values, which corresponds to the incoming light over a defined wavelength range. In hyperspectral imaging typically a few tens to several hundreds of contiguous spectral bands are captured. Typically, researchers use sensors like these on Landsat, SPOT satellites or the Airborne Visible Infrared Imaging Spectrometer (AVIRIS). These sensors provide static information of the Earth's surface and allow static analysis. This area has been firmly established for many years and is essential for several applications like earth observation, inspection and agriculture. But the topic of onboard realtime hyperspectral image analysis for autonomous navigation is relatively unexplored. New sensors and procedures are needed here. A drawback of established approaches are the scanning requirements for constructing a full 3-D hypercube of a scene. Using line-scan cameras, multiple lines need to be scanned, while for cameras using special filters several frames have to be captured to construct an spectral image of the scene. The slow acquisition time is responsible for motion artifacts when observing dynamic scenes. This drawback can be overcome with novel highly compact, low-cost, snapshot mosaic (SSM) imaging. Since this technology can be built in small cameras and the capture time is considerably shorter than that of filter wheel solutions allowing to capture a hyperspectral cube at one discrete point in time. Using this sensors it is possible to install hyperspectral cameras system on unmanned land vehicles and utilize them for terrain classification and autonomous while moving. Due to the specific mosaic structure of these sensors, special preprocessing is needed in order to obtain a hypercube with spectral reflectance from captured the raw data.

In this paper we investigate the use of snapshot mosaic hyperspectral cameras on unmanned land vehicles for drivability analysis utilizing machine learning techniques to classify spectral reflectances. We make use of established supervised classifiers to recognize different classes like drivable, rough and obstacle which can bee seen as terrain recognition or environmental perception based on spectral reflectances.

The remainder of this paper is organized as follows. In the following section an overview of common algorithms for spectral classification is given. Then our general setup and preprocessing is presented in section 3. Our classification approach is described in detail in section 4. And in section 5 we present our results on our new hand-labeled dataset. Finally a conclusion of our work is given in section 6.

Winkens C., Sattler F. and Paulus D.
Hyperspectral Terrain Classification for Ground Vehicles.
DOI: 10.5220/0006275404170424
In *Proceedings of the 12th International Joint Conference on Computer Vision, Imaging and Computer Graphics Theory and Applications (VISIGRAPP 2017)*, pages 417-424
ISBN: 978-989-758-226-4

2 RELATED WORK

Hyperspectral image classification has been under active development recently. Given hyperspectral data, the goal of classification is to assign a unique label to each pixel vector so that it is well-defined by a given class. The availability of labeled data is quite important for nearly all classification techniques. Although there are some unsupervised classification algorithms in literature, we focus on supervised classification for the moment, because it is more widely used as shown by Plaza et al. (Plaza et al., 2009). Most supervised classifiers suffer from the Hughes effect (Hughes, 1968) especially when dealing with high dimensional hyperspectral data. To deal with this issue Melgani et al. (Melgani and Bruzzone, 2004) and Camps-Valls et al. (Camps-Valls and Bruzzone, 2005) introduced support vector maschines with adequate kernels for hyperspectral classifications. SVMs where originally introduced as a binary classifier (Schölkopf and Smola, 2002). So to solve multi-class problems usually several binary classifiers are combined.

Supervised techniques are limited by the availability of labeled training data and suffer from the high dimensionality of the data. While recording data is usually quite straightforward, the precise and correct annotation of the data is very time-consuming and complicated. Therefore Semi-supervised techniques have come up to fix this as proposed by Camps-Valls et al. (Camps-Valls et al., 2011). Jun et al. (Li et al., 2010) presented an semi-supervised classifier that selects non-annotated data based on its entropy and adds it to the training set. The classification of hyperspectral data reveals several important challenges. There is a great mismatch between the high dimensionality of the data in the spectral range, its strong correlation and the availability of annotated data, which are absolutely necessary for the training. Another challenge is the correct combination and integration of spatial and spectral information to take advantage of both of the features.

In various experiments by Li et al. (Li et al., 2012) it was observed that classification-results can be improved by investigating spatial information in parallel with the spectral data. Different efforts have been made to incorporate context-sensitive information in classifiers for hyperspectral data (Plaza et al., 2009). Fauvel et al. (Fauvel et al., 2008) fuse morphological and hyperspectral data to enhance classification results. As a consequence, it has now been widely accepted that the combined use of spatial and spectral information offers significant advantages. To integrate the context into kernel-based classifiers, a pixel can be simultaneously defined both in the spectral domain and in the spatial domain by applying a corresponding feature extraction. Contextual characteristics are defined, for example, by the standard deviation per spectral band. Contextual features are achieved, for example, by the standard deviation per spectral band. This leads to a family of new kernel methods for hyperspectral Data classification reported by Camps-Valls et al. (Camps-Valls et al., 2006) and implemented using an support vector machine.

An alternative approach to combining contextual and spectral information is the use of Markov random fields (MRFs). They exploit the probabilistic correlation of adjacent labels (Tarabalka et al., 2010).

There is already a broad literature base for optical indices in de hyperspectral domain. A study provided by Main et al. (Main et al., 2011), which tested 73 chlorophyll spectral indices on various data sets. The indices were evaluated and ranked based on their prediction error (RMSE). The majority of the most powerful indices were simple ratio or normalized difference indices based on wavelengths outside the chlorophyll absorption center of 680-730 nm. One of these indices is the Normalized Differenced Vegetation Index (NDVI) (Kriegler et al., 1969).

Recently Tsagkatakis et al. (Tsagkatakis et al., 2016; Tsagkatakis and Tsakalides, 2016) proposed several preprocessing methods for reconstruction of spectral data which was captured with the cameras we use. The reconstruction for example is done by utilizing spatio-spectral compressed sensing (Tsagkatakis and Tsakalides, 2015; Tzagkarakis et al., 2016). Whereas Degraux et al. (Degraux et al., 2015) formulate the demosaicing as a 3-D inpainting problem to solve it and increase the resolution of the data volume.

The combination of RGB and multispectral data, using the same hyperspectral snapshot cameras, was evaluated by Cavigelli et al. (Cavigelli et al., 2016) on data with static background and a very small dataset utilizing depp neural nets.

3 SENSOR SETUP

The hyperspectral cameras used here were build by Ximea utilizing a snapshot mosaic filter which has a per-pixel design. The filters are arranged in a rectangular mosaic pattern of n rows and m columns, which is repeated w times over the width and h times over the height of the sensor. For convenience, we call one mosaic pattern a macro pixel, which contains exactly all wavelength sensitivities. In this work we used the MQ022HG-IM-SM4X4-VIS (*VIS*) and the MQ022HG-IM-SM5X5-NIR (*NIR*) cameras man-

(a) Example raw image taken by the *VIS* camera.

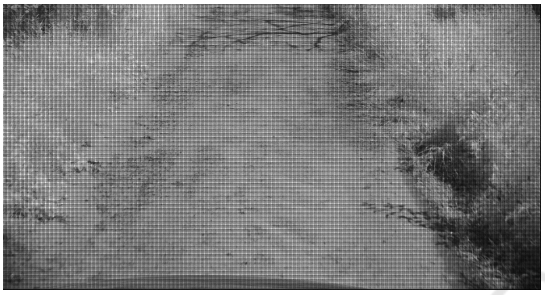

(b) Example raw image taken by the *NIR* camera.

Figure 1: Raw images of *NIR* and *VIS* camera with visible mosaic pattern.

ufactured by Ximea with an an chip from IMEC (Geelen et al., 2014). These sensors are designed to work in specific spectral ranges which are called the active range. The active ranges for these sensors are:

- visual spectrum (*VIS*): 470-620 nm
- near infrared spectrum (*NIR*): 600-1000 nm

This leads to a mosaic pattern with $n_{\text{VIS}} = 4, m_{\text{VIS}} = 4$ for the *VIS* and $n_{\text{NIR}} = 5, m_{\text{NIR}} = 5$ for the *NIR* camera. Ideally every filter has peaks centered around a defined wavelength spectrum with no response outside. However contamination is introduced into the response curve and the signal due to physical constraints. These effects can be summarized as a spectral shift, spectral leaking, and crosstalk and need to be compensated.

The raw data we get from the camera needs a special preprocessing. Therefore we need to obtain a hypercube with spectral reflectance/radiance from the raw data. This step consists of cropping the raw-image to the valid sensor area, removing the vignette and converting to a three dimensional image, also called *hypercube*. Reflectance calculation is the process of extracting the reflectance signal from the captured data of an object. The purpose is to remove the influence of the sensor characteristics like quantum efficiency and the illumination source on the hyperspectral representation of objects.

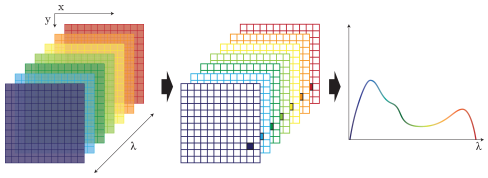

Figure 2: A schematic representation of a hypercube and an interpolated plot of a single data point.

We define a hypercube as

$$\mathcal{H}\colon \mathcal{L}_x \times \mathcal{L}_y \times \mathcal{L}_\lambda \to \mathbb{R} \tag{1}$$

where $\mathcal{L}_x$, $\mathcal{L}_y$ are the spatial domain and $\mathcal{L}_\lambda$ the spectral domain of the image.

Figure 2 shows a visual interpretation of a hypercube.

The hypercube is understood as a volume, where each point $\mathcal{H}(x,y,\lambda)$ corresponds to a spectral reflectance.

Derivated from the above definition a spectrum χ at (x,y) is defined as

$$\mathcal{H}(x,y) = \chi, \tag{2}$$

where $\chi \in \mathbb{R}^{|\mathcal{L}_\lambda|}$ and $|\mathcal{L}_\lambda| = n \cdot m$. The image with only one wavelength, called a spectral band

$$\mathcal{H}(z) = \mathcal{B}_{\lambda=z}, \tag{3}$$

is defined as follows:

$$\mathcal{B}_\lambda : \mathcal{L}_x \times \mathcal{L}_y \to \mathbb{R} \tag{4}$$

This image contains $\mathbf{x} = (x,y)$ the wavelength sensitivity λ for each coordinate.

4 HYPERSPECTRAL CLASSIFICATION

Supervised learning techniques like Random Forest need a training set, which consists of a set of sample feature vectors coupled with a corresponding labeling. The labels $c \in \mathcal{C}$ are user-defined classes which are normally represented by integer numbers. The training and test sets are randomly composed from our annotated dataset, which will be explained in section 5 in more detail.

Given a set of N corresponding training pairs the aim is to find a function γ which generalizes well enough to new data, so accurate predictions for previously unseen data can be calculated.

$$\gamma(\mathbf{x}) = c \tag{5}$$

In this process a classifier might generate a model which is a representation of the given problem from which a classification can be deduced. An accurate

model yields better results for unseen data but highly depends on the training data.

We have chosen to utilize a Random Forest (RF) as a supervised classifier, because it's fast to train and delivers remarkable results.

Random Forests belong to the group of ensemble classifiers and utilize a set of Decision Tree classifiers to learn a robust model. Each classifier is trained on its own subset of training data which is generated by bagging. Bagging is a common approach where samples are randomly drawn with replacement from the original dataset to generate a new distribution of the data. This prevents overfitting and yields different patterns in the input data. The decision trees are unbalanced binary trees. A single decision tree is composed of several nodes, an unique root node, a set of internal nodes and a set of leaves. They form an decision space with the leafs representing a class assignment.

Each of its nodes is composed of a feature index i to split on and a threshold t to split at. It classifies a given feature vector $\mathbf{x}$ as follows. A label is directly assigned if the node is a leaf otherwise a child node assigns the label. The left child node is used if $\mathbf{x}[m] \leq t$ otherwise the right. This recursively partitions the feature space beginning at the unique root node. Building the tree is done also starting at the root by splitting greedily. Splits are calculated by choosing the best feature and the best threshold from all features of the feature vector and a small set of thresholds which is generated randomly. To determine the best split, a gain is maximized. Measurement for the gain G of a split is the weighted impurity $i(\mathbf{x})$ difference between the samples at a node and after the split

$$\mathrm{G} = \mathrm{I}(X) - \sum_{i \in (l,r)} \frac{|X_i|}{|X|} \mathrm{I}(X_i) \tag{6}$$

where X is the given set of feature vectors and X_l/X_r is the set of vectors which is splitted to the left or right. We used the gini impurity for its fast computation and good results. Furthermore these decision trees only use a random subset of the features for every decision node to further increase their diversity. These decision trees, form a Random Forest, which are used to classify the generated subsets. The result of the classification is obtained by majority voting.

In order to classify regions of an environment for its drivability, a suitable model must be trained using a Random Forest classifier. Since two cameras with different wavelength sensitivities were used here, two separate models need to be trained. However, the recorded raw images must first be preprocessed in order to filter error-prone data and then be annotated. Since the data was taken from a vehicle driving in a natural environment with sunlight, they are partially under and overexposed. Therefore, these data must first be sorted out and filtered so that a stable model can be learned. As already mentioned in section 3, a pre-processed image forms a hypercube with a spectrum of 16 or 25 spectral reflectances for each pixel defined as χ. For training, the annotated hypercubes are first dissected and filtered as described above. The remaining spectra are randomly composed to test and training data sets. As input data, a Random Forest now receives an annotated spectrum which consists of a 16 or 25 dimensional feature vector.

Utilizing the training set we trained a Random Forest with ten trees for every camera. By making use of parallelization we were able to further boost the performance of the already fast Random Forest classifier. To solely test the hyperspectral classification accuracy only one spectrum χ with $|\mathcal{L}_\lambda|$ spectral bands has to be given to the classifier at once. This corresponds to a per pixel classification of an image, as further discussed in the next section.

5 EVALUATION

As far as we know, there is no publicly available data set with hyperspectral data recorded by these special cameras. Therefore we built our own dataset, which will be published in the near future. We equipped a standard car with the MQ022HG-IM-SM4X4-VIS (*VIS*) and MQ022HG-IM-SM5X5-NIR (*NIR*) from Ximea. The cameras are calibrated and synchronized using a hardware trigger. We collected a total of $\approx$ 200 GB of data driving through suburban areas, from which we selected a subset for labeling hyperspectral data. As there is no labeling tool, which is able to handle our hyperspectral data correctly, we developed our own.

The recorded and preprocessed data had then to be annotated. This was done by hand for all images of each dataset. During the labeling process not all image pixels have been assigned classes. This is due to the fact, that border areas between materials are not unambiguously assignable. And as later results have shown no errors arised from this constrain. The dataset was labeled in terms of drivability. The main classes were drivable, rough and obstacle furthermore the class sky was introduced as an additional class, because it is an important part of our scene and defines the border of the terrain. Furthermore it's reflectance is visible many places like cars. In addition a principal component analysis (PCA) was performed on this dataset projecting it to 7 features.

Random Forests and Gaussian Naive Bayes (Chan

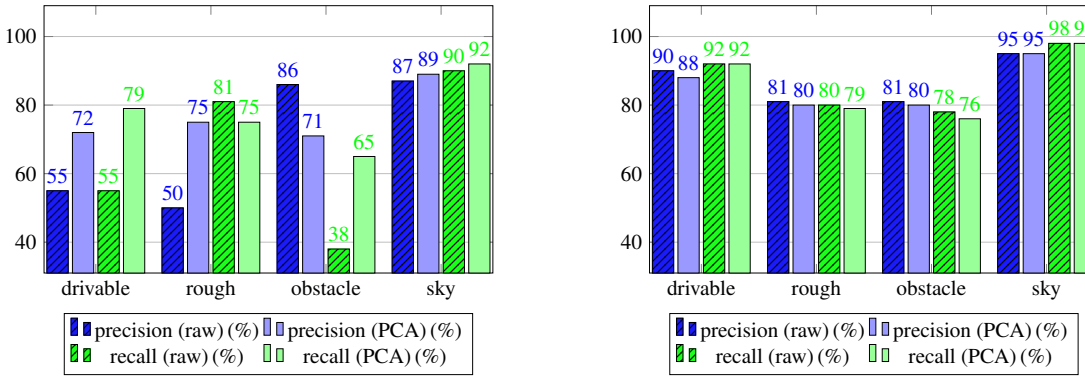

(a) Gaussian Naive Bayes.

(b) Random Forest.

Figure 3: Classification results of Gaussian Naive Bayes and Random Forest on raw and PCA data of the *VIS*-Camera.

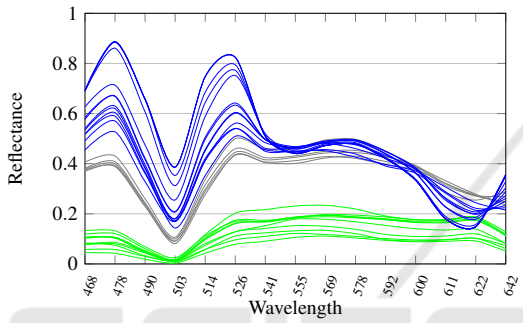

(a) Plots of spectra captured with the *VIS*-Camera. Sky (blue) street (gray) and vegetation (green).

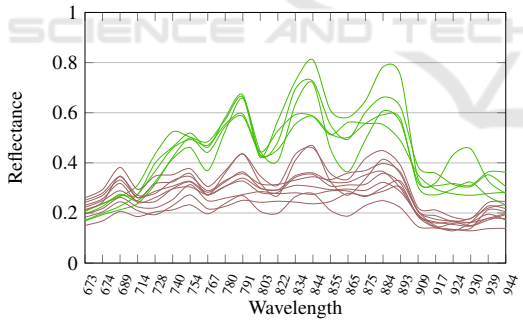

(b) Plots of spectra captured with the *NIR*-Camera. Street (gray) and vegetation (green).

Figure 4: Spectral plots of *NIR*-Camera and *VIS*-Camera for different materials.

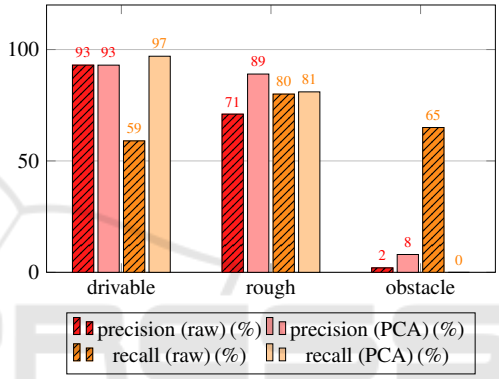

(a) Gaussian Naive Bayes.

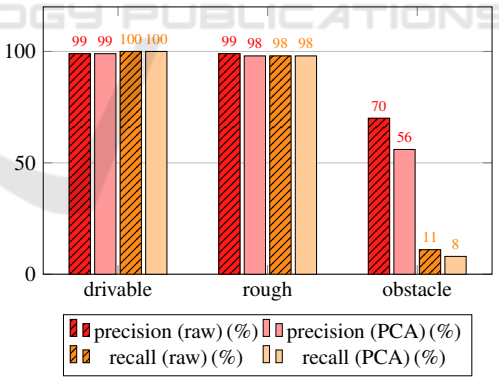

(b) Random Forest.

Figure 5: Classification results of Gaussian Naive Bayes and Random Forest on raw and PCA data of the *NIR*-Camera.

et al., 1982) have been applied to our initial training and test datasets as well as the PCA transformed data.

It is noticeable that the Random Forest classifier has generally produced poorer results with models trained by using PCA data. This is consistent with the findings of Cheriyadat (Cheriyadat and Bruce, 2003), because of the fact that hyperspectral data is highly correlated. The the Gaussian Naive Bayes classifier (GNB) in contrast, produced better results with the PCA as indicated in figure 3. This is justified by the fact that the GNB does not regard the data as being correlated. However, since the spectral data are highly correlated, this classifier does not perform well as a consequence. The PCA implicitly introduces a decorrelation of the data, helping the GNB.

In figure 4 several spectras of classes we recon-

(a) Classification results of *NIR* data captured with the *NIR*-camera on a field track.

(b) Classification results of *NIR* data captured with the *VIS*-camera on a rough field track.

(c) Classification results of *VIS* data captured with the *VIS*-camera on a country road.

(d) Classification results of *VIS* data captured with the *VIS*-camera on a field track.

Figure 6: Results of our classification based on Random Forest trained with our *NIR* and *VIS* data set. The left image shows a single spectrum, the middle is a visualisation of our annotation and the right image shows the visualized classification results.

structed are plotted, were clear differences in the spectral reflectances of the individual classes can be spotted. Furthermore figure 6 shows some visualisations of our classification results. The classifier was able to separate the road cleanly from rough ground and obstacles. Figure 3 and figure 5 provide a more detailed overview of the results. Here the accuracy and precision are plotted against the respective classes.

VIS. The *VIS* camera has a 5 mm lens and a fairly wide field of view and does not only capture the terrain but also the scene above. By looking at figure 3 it is striking that for all classifiers the class sky is by far the highest. This can simply be explained by the fact that the sky in the *VIS* data generally occupies a large area. So enough records are available and the classifier can adapt well. Furthermore, the sky has a very characteristic radiation. Therefore it is very easy to distinguish sky from other areas in the scenery. The Random Forest classifier also produced noticeable high scores for the other classes where rough and obstacle have slightly lower scores. This might be caused by the fact, that the classification uses only spectral information, which can't distinguish between a stone wall and a stone path. Because it isn't trained to take context and spatial information into account. Overall the GNB scores worse with the exception of the raw precision for obstacles.

NIR. First it must be noted that the *NIR* camera, unlike the *VIS* camera, has a double-telecentric 16 mm

lens and is directed downwards. Therefore, it has only recorded data from the road ahead of the vehicle. This means that no data from the sky is available and consequently can not be trained. Furthermore, the training and test data set consists of only about 0.66% of data annotated as an obstacle. Accordingly, the trained model is not capable of classifying obstacles. This is also indicated in figure 5a where Gaussian Naive Bayes is not capable of classifying obstacles. The Random Forest classifier, performed best with a precision of 70% and a recall of 56% on the obstacle class. This suggests that 70% of the data identified as an obstacle was actually an obstacle and 56% of all obstacles were also classified. This is quite remarkable considering the available data.

The classes drivable and rough produced better classification rates. This is because solid ground, which is composed of asphalt or stones, was regarded as being drivable. And meadows, fields, bushes and grasses were labeled as rough. So the rough surface consists almost exclusively of elements, which contain a high proportion of chlorophyll. Elements with chlorophyll are easily separated from elements with a low content of chlorophyll, since chlorophyll has its strongest absorption at about 675 nm and the absorption decreases sharply afterwards, which can be also seen in our reconstructed spectrum in figure 4b.

6 CONCLUSION

The experiments carried out imply a Random Forest classifier to be reliable for hyperspectral classification in combination with the snapshot hyperspectral cameras. The Random Forest classifier delivers decent results for the *NIR* camera as well as for the *VIS* camera. Based on the captured hyperspectral data we were able to precisely distinguish road or drivable areas from non-drivable areas like rough or obstacles, which could greatly enhance terrain classification performance.

Furthermore, a Random Forest can be trained in a short time in comparison to the other methods. Due to its structure, it can be parallelized very well and accelerated effectively. Another interesting result is that the balance of the training is vital for the quality of the classification. These promising results are a first showcase for the capabilities of the novel sensor system and its suitability for terrain classification, e.g. in autonomous driving. In order to improve the pixel-wise classification, we plan to combine it with a conditional random field and to additionally add spatial and laser data to achieve an improved classification.

ACKNOWLEDGEMENTS

This work was partially funded by Wehrtechnische Dienststelle 41 (WTD), Koblenz, Germany.

REFERENCES

Camps-Valls, G. and Bruzzone, L. (2005). Kernel-based methods for hyperspectral image classification. *IEEE Transactions on Geoscience and Remote Sensing*, 43(6):1351–1362.

Camps-Valls, G., Gomez-Chova, L., Muñoz-Marí, J., Vila-Francés, J., and Calpe-Maravilla, J. (2006). Composite kernels for hyperspectral image classification. *IEEE Geoscience and Remote Sensing Letters*, 3(1):93–97.

Camps-Valls, G., Tuia, D., Gómez-Chova, L., Jiménez, S., and Malo, J. (2011). Remote sensing image processing. *Synthesis Lectures on Image, Video, and Multimedia Processing*, 5(1):1–192.

Cavigelli, L., Bernath, D., Magno, M., and Benini, L. (2016). Computationally efficient target classification in multispectral image data with deep neural networks. In *SPIE Security+ Defence*, pages 99970L–99970L. International Society for Optics and Photonics.

Chan, T. F., Golub, G. H., and LeVeque, R. J. (1982). Updating formulae and a pairwise algorithm for computing sample variances. In *COMPSTAT 1982 5th Symposium held at Toulouse 1982*, pages 30–41. Springer.

Cheriyadat, A. and Bruce, L. M. (2003). Why principal component analysis is not an appropriate feature extraction method for hyperspectral data. In *Geoscience and Remote Sensing Symposium, 2003. IGARSS'03. Proceedings. 2003 IEEE International*, volume 6, pages 3420–3422. IEEE.

Degraux, K., Cambareri, V., Jacques, L., Geelen, B., Blanch, C., and Lafruit, G. (2015). Generalized inpainting method for hyperspectral image acquisition. In *Image Processing (ICIP), 2015 IEEE International Conference on*, pages 315–319. IEEE.

Fauvel, M., Benediktsson, J. A., Chanussot, J., and Sveinsson, J. R. (2008). Spectral and spatial classification of hyperspectral data using svms and morphological profiles. *IEEE Transactions on Geoscience and Remote Sensing*, 46(11):3804–3814.

Geelen, B., Tack, N., and Lambrechts, A. (2014). A compact snapshot multispectral imager with a monolithically integrated per-pixel filter mosaic. In *Spie Moems-Mems*, pages 89740L–89740L. International Society for Optics and Photonics.

Hughes, G. (1968). On the mean accuracy of statistical pattern recognizers. *IEEE transactions on information theory*, 14(1):55–63.

Kriegler, F., Malila, W., Nalepka, R., and Richardson, W. (1969). Preprocessing transformations and their effects on multispectral recognition. In *Remote Sensing of Environment, VI*, volume 1, page 97.

Li, J., Bioucas-Dias, J. M., and Plaza, A. (2010). Semisupervised hyperspectral image segmentation using multinomial logistic regression with active learning. *IEEE Transactions on Geoscience and Remote Sensing*, 48(11):4085–4098.

Li, J., Bioucas-Dias, J. M., and Plaza, A. (2012). Spectral–spatial hyperspectral image segmentation using subspace multinomial logistic regression and markov random fields. *IEEE Transactions on Geoscience and Remote Sensing*, 50(3):809–823.

Main, R., Cho, M. A., Mathieu, R., OKennedy, M. M., Ramoelo, A., and Koch, S. (2011). An investigation into robust spectral indices for leaf chlorophyll estimation. *ISPRS Journal of Photogrammetry and Remote Sensing*, 66(6):751–761.

Melgani, F. and Bruzzone, L. (2004). Classification of hyperspectral remote sensing images with support vector machines. *IEEE Transactions on geoscience and remote sensing*, 42(8):1778–1790.

Plaza, A., Benediktsson, J. A., Boardman, J. W., Brazile, J., Bruzzone, L., Camps-Valls, G., Chanussot, J., Fauvel, M., Gamba, P., Gualtieri, A., et al. (2009). Recent advances in techniques for hyperspectral image processing. *Remote sensing of environment*, 113:S110–S122.

Schölkopf, B. and Smola, A. J. (2002). *Learning with kernels: support vector machines, regularization, optimization, and beyond*. MIT press.

Tarabalka, Y., Fauvel, M., Chanussot, J., and Benediktsson, J. A. (2010). Svm-and mrf-based method for accurate classification of hyperspectral images. *IEEE Geoscience and Remote Sensing Letters*, 7(4):736–740.

Tsagkatakis, G., Jayapala, M., Geelen, B., and Tsakalides, P. (2016). Non-negative matrix completion for the enhancement of snap-shot mosaic multispectral imagery.

Tsagkatakis, G. and Tsakalides, P. (2015). Compressed hyperspectral sensing. In *SPIE/IS&T Electronic Imaging*, pages 940307–940307. International Society for Optics and Photonics.

Tsagkatakis, G. and Tsakalides, P. (2016). A self-similar and sparse approach for spectral mosaic snapshot recovery. In *2016 IEEE International Conference on Imaging Systems and Techniques (IST)*, pages 341–345.

Tzagkarakis, G., Charle, W., and Tsakalides, P. (2016). Data compression for snapshot mosaic hyperspectral image sensors.